View metadata, citation and similar papers at core.ac.uk
brought to you by CORE
provided by Wood and Fiber Science (E-Journal)

MICROSTRUCTURE AND ADSORPTION PROPERTY OF BAMBOO-BASED ACTIVATED CARBON FIBERS PREPARED BY LIQUEFACTION AND CURING

*Xiaojun Ma**
Associate Professor
E-mail: mxj75@tust.edu.cn

Xinyan Liu
Lecturer
E-mail: liuxianyan@tust.edu.cn

Lili Yu†
Lecturer
E-mail: yulilucky@tust.edu.cn

Min Tian
Graduate Student
Department of Wood Science and Technology
Tianjin University of Science & Technology
Tianjin 300222, China
E-mail: tianmin@tust.edu.cn

(Received August 2013)

Abstract. In this study, activated carbon fibers (BACF) were prepared from moso bamboo by phenol liquefaction, spinning, curing, and CO_2 activation. The microstructure and porous texture of BACF were investigated by Fourier transform IR spectroscopy, X-ray diffraction, and N_2 adsorption at –196°C. The surface area and pore volume increased progressively after activation, and yields were found in the range of 39-59.6%. BACF showed type I isotherms with multimodal pore size distributions in the <6-nm region. It is believed that liquefied bamboo could be a suitable precursor for activated carbon fibers. The obvious change was not observed on the functional groups of BACF during activation. At the same time, it was found that the higher temperature improved the crystallite size and activation reaction of BACF.

Keywords: Bamboo, activated carbon fibers, adsorption, microstructure, porosity.

INTRODUCTION

Because of uniform slit-shaped micropores and great surface area, activated carbon fibers (ACF) have been widely applied for purification, separation, or catalysis (Fan et al 2004). Currently, ACF are mainly prepared from polyacrylonitrile, phenolic resin, or pitch fibers (Li et al 1998; Ryu et al 2002; Tan et al 2007). The shortage of these resources necessitates an improvement in ACF production, which highly depends on chemical materials. With the increase of fossil fuel shortage and environmental protection, developing renewable biomass-based ACF is particularly important.

During the last few decades, biomass-based ACF have been prepared from wood, kenaf, jute, coconut, etc (Uraki et al 2001; Asakura et al 2004; Ngoc et al 2006; Cuerda-Correa et al 2008; Rong et al 2010). However, most studies on preparation of ACF with biomass only partly use biomass constituents such as cellulose and lignin. The utilization ratio of biomass materials for ACF is quite low. Recently, biomass materials

* Corresponding author
† SWST member

© 2014 by the Society of Wood Science and Technology

have been completely converted into useful chemical raw by a liquefaction technique, and liquefaction products have been used to prepare adhesives, foam, wood, ceramics, carbon fibers, etc (Masahiko et al 2004; Lin et al 2006). It greatly improves the use of these materials and provides a new method for the preparation of biomass-based ACF.

Bamboo is known as a cheap and fast-grown resource that offers great potential as an alternative to wood. In previous work, we carried out the preparation of carbon fiber from liquefied wood instead of fossil sources (Ma and Zhao 2010). ACF could be prepared from liquefied wood or bamboo-based carbon fiber by activation technology. However, the adsorption capacity of ACF depends on many factors, such as raw materials, activation process, pore structure, and surface functionalities. During the activation, pore development of ACF is caused by the enhanced activation reactions between carbon and activating agents at appropriate temperature. Also, the different precursors would give the final products different properties of ACF. Therefore, it is significant to study the activation technology of ACF from liquefied bamboo.

In this study, based on previous studies, activated carbon fibers (BACF) were prepared from bamboo after phenol liquefaction, melt spinning, curing, and activation using CO_2. At the same time, to investigate the influences of activation temperature on the structure and performance of BACF, the microstructure, adsorption capacity, and porous distribution of BACF were also studied in detail.

MATERIALS AND METHODS

Preparation of Bamboo-Activated Carbon Fibers

The mixture of moso bamboo powder (20-80 mesh), phenol (1:6 mass proportion), and 8% phosphoric acid was liquefied for 2.5 h at 160°C. The bamboo liquefaction was mixed with 5% synthetic hexamethylenetetramine (based on the mass percentage of the liquefied product) in a spinning machine to synthesize the fed material into the spinning solution at 130°C. The spinning solution was used to form the initial fiber using the melt spinning process. The initial fiber was placed in a hydrochloric acid–formaldehyde mixture solution with a hydrochloric acid concentration of 18.5% and formaldehyde concentration of 18.5%. The mixture was subjected to solidification for 4 h at 95°C. The initial fiber was rinsed and then placed in a box to dry for 40 min at 90°C to obtain the precursor fiber (YS).

The precursor fiber was placed in a carbonizing-activating furnace with N_2 at a flow rate of 100 mL/min. The fiber was heated evenly by raising the temperature in increments of 5°C/min until the set activation temperature was reached. Finally, 600 mL/min of CO_2 was fed for 40 min to activate the fiber and until BACF was obtained.

Characterization of Bamboo-Activated Carbon Fibers

Surface morphologies of BACF were examined using a scanning electron microscope (SEM) (SS-550; Shimadzu, Kyoto, Japan) with an acceleration voltage of 15 kV. Prior to imaging, all samples were sputtercoated with gold and then mounted on the SEM stage.

The crystal structures of BACF were measured by a powder X-ray diffractometer (D/max-2500; Rigaku, Tokyo, Japan) using Cu Kα radiation ($\lambda = 0.154$ nm, powdery samples) and a diffraction angle range of $2\theta = 5\text{-}60^\circ$ with a count time of 20 s at each point. The accelerating voltage and applied current were 40 kV and 100 mA, respectively.

To examine the differences of microcrystalline structure of BACF at various temperatures, the apparent crystallite thickness (L_c), the apparent layer-plane length parallel to the fiber axis

(L_a), and the average interlayer spacing d were calculated using Scherrer and Bragg's equations. The formulas can be expressed as

$$d = \frac{\lambda}{2\sin\theta} \quad (1)$$

$$L = \frac{K\lambda}{\beta\cos\theta} \quad (2)$$

where θ is the Bragg angle of peaks (°), λ is the wavelength of X-ray used (0.154 nm), and β is half-height width of peak (rad). The form factor K is 0.89 for L_c and 1.84 for L_a, respectively (Johnson and Frank 1980).

The chemical characterization of functional groups of BACF was detected using pressed potassium bromide (KBr) pellets containing 5% of sample by Fourier transform IR spectrometry (FTIR) (Nicolet-6700; Thermo electron, Waltham, MA) in the scanning range of 4000-400 cm^{-1}. The samples were pulverized (150-200 mesh) and mixed with KBr before being pressed into a disk.

Specific surface area was obtained from a nitrogen adsorption–desorption isotherm taken at –196°C with an ASAP-2020 (Micromeritics Instrument Corporation, Norcross, GA). The surface area of each specimen was obtained based on the Brunauer–Emmett–Teller (BET). The micropore area and micropore volume were calculated by the t-plot method. The pore size distributions were obtained based on the Horvath–Kawazoe (HK) method for micropores and the Barrett–Joyner–Halenda (BJH) method for mesopores. Total pore volume and radius were based on the assumption that nitrogen filled the sample pores at a relative pressure of 0.99 (Carrott et al 1987).

Iodine and methylene blue (MB) adsorption were calculated following the GB/T 12496.8 (GB 1999a) standard test method for granular activated carbon from wood of iodine adsorption and the GB/T 12496.10 (GB 1999b) standard test method for granular activated carbon from wood of MB adsorption.

RESULTS AND DISCUSSION

Morphological Characteristics

Figure 1 shows the SEM image of the surface and cross-section of BACF. Figure 1a-b shows that the surface of BACF is smooth with no obvious pores. Figure 1c-d shows that some relatively large pores existed at the edge of the section primarily because the gas generated during spinning was not fully exhausted.

Iodine, Methylene Blue Adsorption, and Yield

Figure 2 shows the iodine, MB adsorption, and yield rate curves of BACF in different activation temperatures. As shown in Fig 2a, with increased activation temperature, iodine and MB adsorption of BACF gradually increased. Iodine and MB adsorption values of BACF increased slowly in the activation temperature range of 500-700°C, whereas iodine and MB adsorption values increased significantly when temperature exceeded 700°C and improved 268.4 and 629.6%, respectively, indicating that the main pore formation period of BACF occurs in the range of 700-900°C. In addition, it was observed that the adsorption growth of MB was significantly higher than that of iodine, indicating that the mesopores of BACF became more and more numerous at temperatures exceeding 700°C.

As shown in Fig 2b, with increased activation temperature, the yield rate of BACF gradually decreased. The final carbonization temperature plays an important role in the yield of BACF. When the temperature was below 800°C, the yield slowly decreased. In contrast, when the temperature exceeded 800°C, the yield significantly decreased. It is clear that higher activation temperature enhances the reaction of the activating agent with carbon. The yield rate of BACF decreased from 59.6 to 39% as temperature

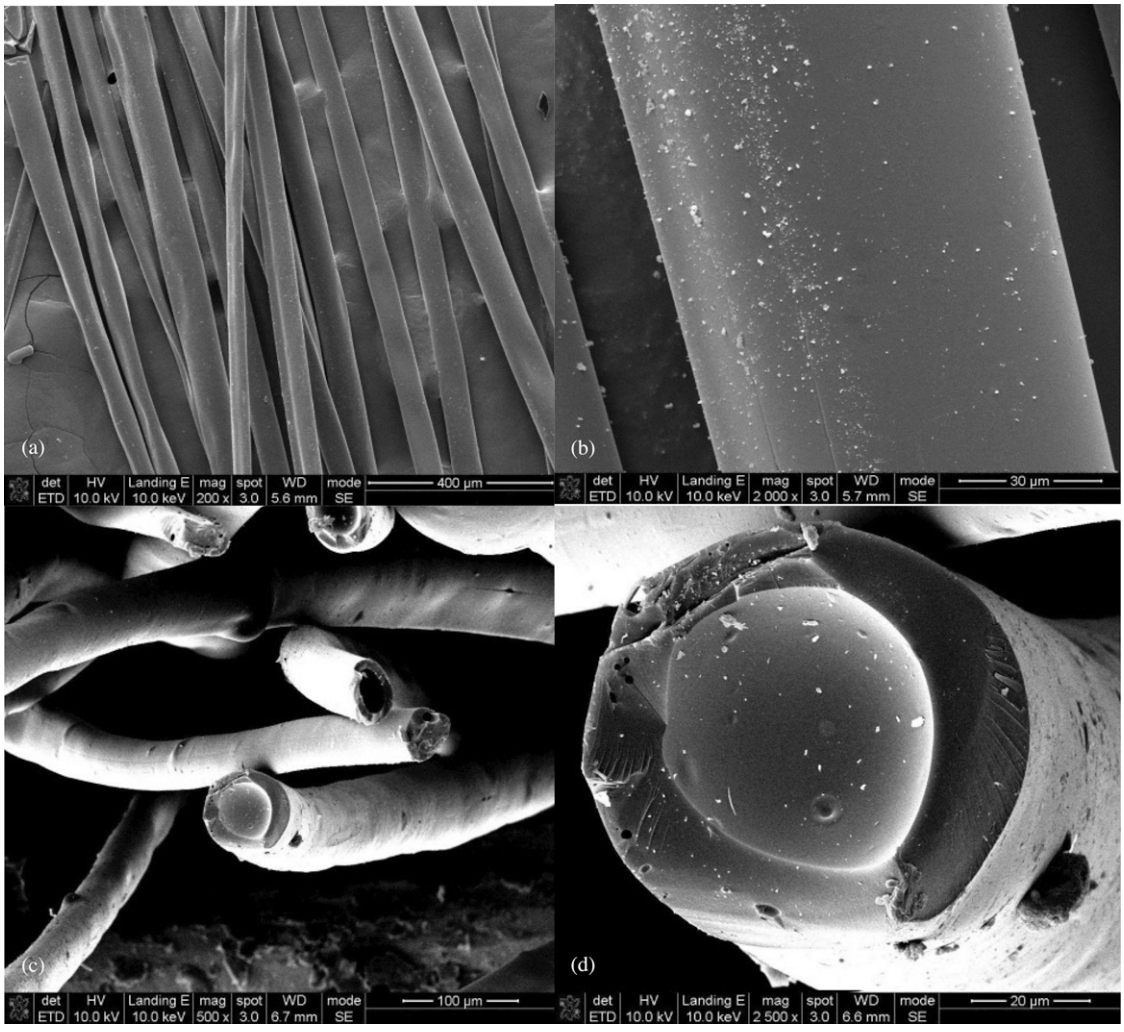

Figure 1. Scanning electron microscope photographs of activated carbon fibers from bamboo. (a-b) Side surface; (c-d) cross-section.

increased from 500 to 900°C. It is clear that the yield of BACF was higher than that of biomass-based activated carbon fibers reported (Uraki et al 2001; Asakura et al 2004).

X-Ray Diffraction Analysis

Figure 3 shows X-ray diffraction (XRD) patterns of BACF at various activation temperatures. With increased activation temperature, the 002 peak began to shift toward a higher angle and became broader, corresponding to smaller-sized crystallites. Above 600°C, the samples presented (100) diffraction peak ($2\theta = 43°$). Finally, X-ray diffractograms for BACF showed a similar diffraction pattern, denoting that these fibers were less crystalline than the graphite, although they still maintained a certain order for the graphene layers. Table 1 shows the XRD structure parameters of BACF under various activation temperatures calculated based on the Scherrer and Bragg formulas. With increased activation temperature, the value of $d_{(002)}$ gradually decreased, whereas

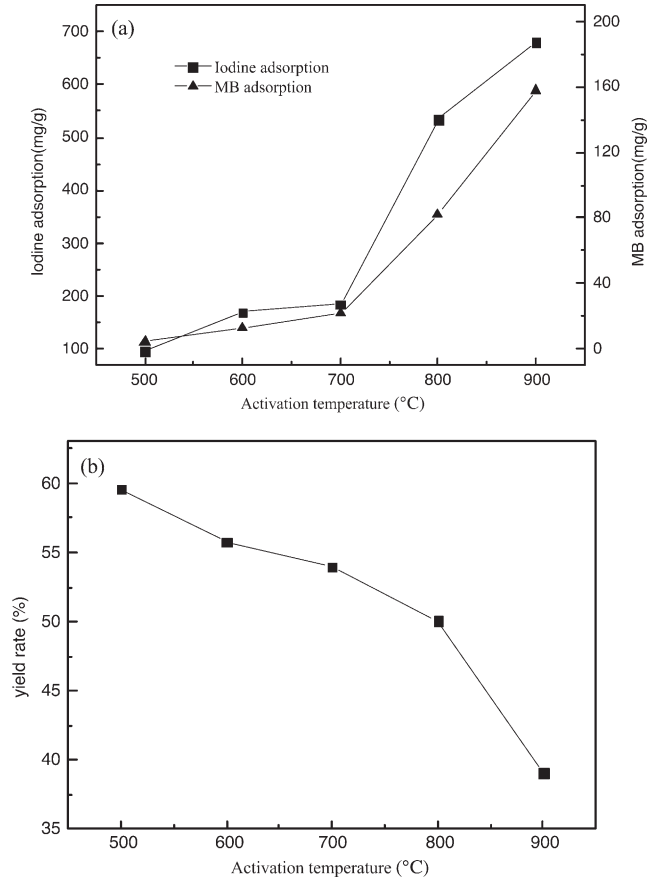

Figure 2. Iodine, methylene blue (MB) adsorption (a) and yield rate (b) of activated carbon fibers from bamboo at various temperatures.

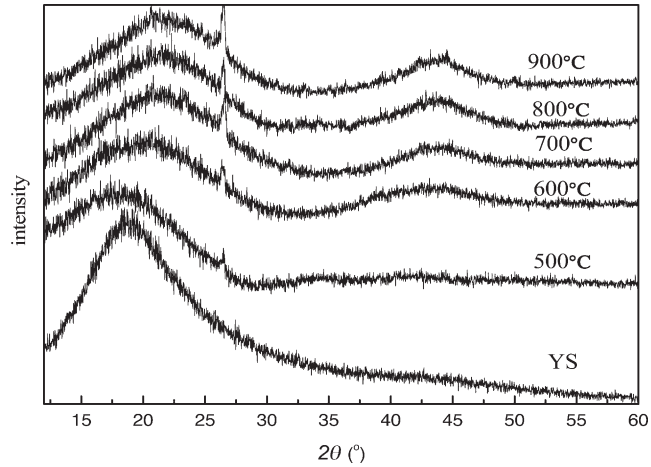

Figure 3. X-ray diffraction of the bamboo precursor fiber (YS) and activated carbon fibers from bamboo at various temperatures.

Table 1. Structure parameters of X-ray diffraction for activated carbon fibers from bamboo.

Temperature (°C)	$d_{(002)}$ (nm)	L_c (nm)	L_a (nm)	$L_c/d_{(002)}$
500	0.4949	0.5959	1.2320	1.2040
600	0.4479	0.7054	1.4584	1.5751
700	0.4147	0.7804	1.6135	1.8818
800	0.4109	0.8388	1.7343	2.0414
900	0.4035	0.8155	1.6859	2.0208

the values of the crystallite sizes L_a, L_c, and $L_c/d_{(002)}$ increased. It indicates that with the increase in temperature, the crystallite size of BACF gradually approached that of graphite and became orderly (Kercher and Nagle 2003; Maciá-Agulló et al 2007).

Fourier Transform IR Analysis

To identify the variation of functional groups during formation of BACF from source materials, IR spectrum analysis was performed to check out the types of organic groups presenting on the surface of raw materials and prepared BACF. Figure 4 shows FTIR of the bamboo precursor fiber (YS) and BACF at various activation temperatures. When the activation temperature increased from 500 to 700°C, the characteristic vibrations of O-H at 3436 cm^{-1}, C-H at 2895-2856 cm^{-1}, C=C at 1629-1598 cm^{-1}, C-O at 1263-1043 cm^{-1}, and C-H out-of-plane of benzene ring at 900-650 cm^{-1} did not change significantly (Burg et al 2002; Olivares-Marín et al 2006). However, above 700°C, the intensity of the band at 1263-1043 cm^{-1}, corresponding to C-O stretching, became obvious, indicating that it is beneficial for high temperature to improve the activation reaction of BACF. At the same time, it was found that the activation temperature played an important role on structure symmetry formation in the CO_2 activation process.

Nitrogen Adsorption

Figure 5 shows nitrogen adsorption–desorption isotherms of BACF at various activation temperatures. As can be seen in Fig 5, at low relative pressures, a rapid increase in the adsorption–desorption isotherms was observed, which was followed by a nearly horizontal plateau at higher relative pressures, indicating the isotherms of BACF belonged to type I in the IUPAC classification (Sing et al 1985). The type I isotherm represents a material with microporous structure. The major uptake occurs at low relative pressures indicating the formation of highly porous materials with narrow pore size distribution. The steep rise and very high N_2

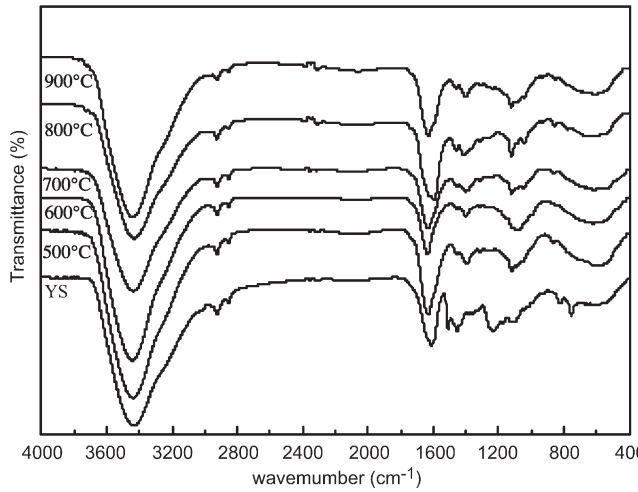

Figure 4. Fourier transform IR spectroscopy of the bamboo precursor fiber (YS) and activated carbon fibers from bamboo at various temperatures.

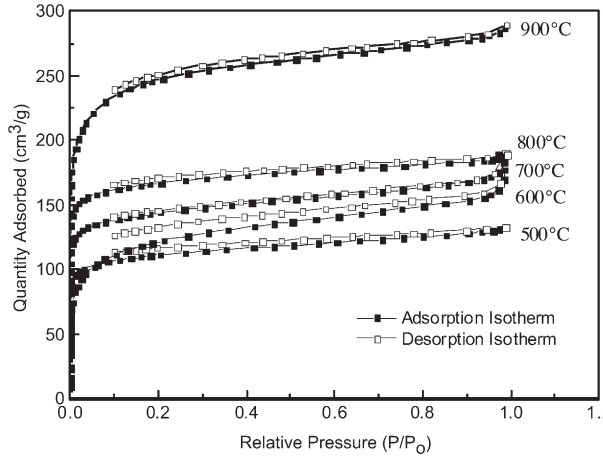

Figure 5. Nitrogen adsorption–desorption isotherm plots for activated carbon fibers from bamboo.

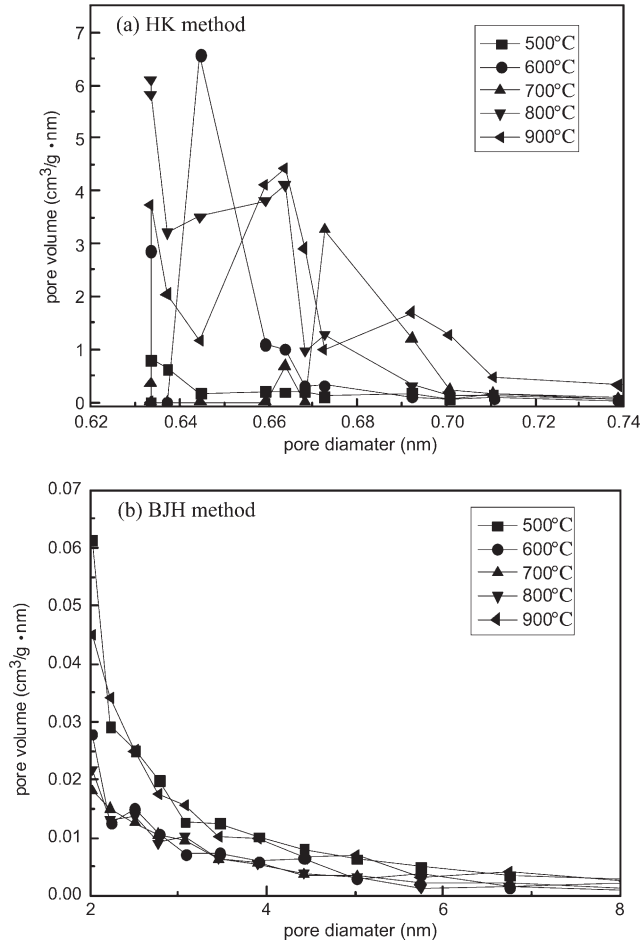

Figure 6. Pore size distribution of activated carbon fibers from bamboo at various temperatures: (a) Horvath–Kawazoe (HK) method; (b) Barrett–Joyner–Halenda (BJH) method.

Table 2. Surface areas and pore volumes of activated carbon fibers from bamboo at various temperatures.[a]

Temperature (°C)	S_{BET} (m^2/g)	S_{mic} (m^2/g)	S_{mes} (m^2/g)	V_{tot} (cm^3/g)	V_{mic} (cm^3/g)	V_{mes} (cm^3/g)	V_{mic} (%)
500	365.5	169.9	72.8	0.2057	0.0776	0.0338	37.7
600	375.9	269.4	57.6	0.2238	0.1259	0.0386	56.3
700	405.7	300.5	46.3	0.2458	0.1397	0.0767	56.8
800	430.4	338.6	35.1	0.2541	0.1580	0.0775	62.2
900	702.3	451.9	32.6	0.3234	0.2099	0.0992	64.9

[a] S_{BET}, Brunauer–Emmett–Teller surface area; S_{mic}, micropore surface area; S_{mes}, mesopore surface area; V_{tot}, total pore volume; V_{mic}, micropore volume; V_{mes}, mesopore volume; $V_{mic}\% = (V_{mic}/V_{tot}) \times 100$.

uptake of the initial part of the isotherms suggest the presence of a large proportion of micropores and the fact that no obvious hysteresis was observed indicates that the amount of mesopores or macropores was very small (Yang et al 2012).

During activation, the activating agent reacts with the reactive centers such as disorganized carbons, carbons with heteroatom, and carbons on graphene edges, creating new pores and widening the existing ones. The pore development of carbon is caused by the enhanced activation reactions between carbon and activating agents at appropriate temperature. Figure 6 shows the pore size distribution (HK and BJH methods) of BACF at different temperatures. According to the pore size distribution shown using the HK method in Fig 6a, samples obtained at low activation temperature such as 500-600°C were predominantly microporous with pore width <0.66 nm. With temperature increased to 900°C, the pores mainly distributed in the range <0.71 nm. The micropore sizes of BACF distributed mainly between 0.6 and 0.7 nm during activation. According to Fig 6b, with increasing activation temperature, mesopores occurred, and the mesopore sizes mainly distributed in the range 2-6 nm.

Table 2 gives the surface areas and pore volumes of BACF at various activation temperatures. The S_{BET}, S_{mic}, and pore volumes of BACF gradually increased with increase in activation temperature. When the final carbonization temperature was raised to 900°C, S_{BET}, S_{mic}, and S_{mes} were 702.3, 451.9, and 32.6 m^2/g, respectively, and V_{tot}, V_{mic}, and V_{mes} were 0.3234, 0.2099, and 0.0992 cm^3/g, respectively. As Table 2 shows, the microporosity also changes with increasing carbonization temperature. Microporosity increased from 37.7 to 64.9% as temperature increased from 500 to 900°C. According to the obtained results, the greatest surface area and total pore volume of BACF were developed by a further rise in activation temperature, and it is suggested that 900°C would be the most suitable temperature.

There are some references in the literature to bamboo-based activated carbons despite the encouraging results reported in this study. Previous work reported surface area values around 400-500 m^2/g (Mizuta et al 2004; Asada et al 2006) for bamboo carbons. Table 2 shows that the S_{BET} of BACF were higher than those previously reported. It is believed that liquefied bamboo materials could be a suitable precursor for activated carbon fibers.

CONCLUSIONS

Bamboo-based activated carbon fibers prepared by liquefaction had high surface area and a complex pore structure. As the activation temperature rose, the crystallite size $d_{(002)}$ gradually became small, whereas L_a, L_c, and $L_c/d_{(002)}$ gradually increased. The crystallite size and activation reaction of bamboo-based activated carbon fibers were highly dependent on activation temperature. The maximum iodine and MB absorption of BACF were 679.91 and 157.83 $mg \cdot g^{-1}$, respectively. Bamboo-based activated carbon fibers with BET surface area of 702.3 m^2/g were obtained at 900°C, and yields of 50% below 800°C could be achieved by activation for 40 min. The pore size of BACF was mainly

0.6- to 0.7-nm micropores, but small mesopores of 2-6 nm also made an important contribution. This will lead to the development of bamboo-based activated carbon with different pore sizes. Finally, it is believed that liquefied biomass materials could be a suitable precursor for activated carbon fibers.

ACKNOWLEDGMENTS

This research was financially supported by the National Natural Science Foundation of PR China (No. 31270607).

REFERENCES

Asada T, Ohkubo T, Kawata K, Oikawa K (2006) Ammonia adsorption on bamboo charcoal with acid treatment. J Health Sci 52(5):585-589.

Asakura R, Morita M, Maruyama K, Hatori H, Yamada Y (2004) Preparation of fibrous activated carbons from wood fiber. J Mater Sci 39(1):201-206.

Burg P, Fydrych P, Cagniant D, Nanse G, Bimer J, Jankowska A (2002) The characterization of nitrogen-enriched activated carbons by IR, XPS and LSER methods. Carbon 40(9):1521-1531.

Carrott PJM, Roberts RA, Sing KSW (1987) Standard nitrogen adsorption data for nonporous carbons. Carbon 25(6):769-770.

Cuerda-Correa EM, Macías-García A, Díaz Díez MA, Ortiz AL (2008) Textural and morphological study of activated carbon fibers prepared from kenaf. Microporous Mesoporous Mater 111(3):523-529.

Fan M, Marshall W, Daugaard D, Brown RC (2004) Steam activation of chars produced from oat hulls and corn stover. Biores Technol 93(1):103-107.

GB (1999a) T 12496.8. Test method of wooden activated carbon—Determination of iodine number. Beijing, China.

GB (1999b) T 12496.10. Test method of wooden activated carbon—Determination of methylene blue adsorption. Beijing, China.

Johnson DJ, Frank C (1980) Recent advances in studies of carbon fibre structure. Transactions of the Royal Society A 294(1411):443-449.

Kercher AK, Nagle DC (2003) Microstructural evolution during charcoal carbonization by X-ray diffraction analysis. Carbon 41(1):15-27.

Li CY, Wan YZ, Wang J, Wang YL, Jiang XQ, Han LM (1998) Antibacterial pitch-based activated carbon fiber supporting silver. Carbon 36(1-2):61-65.

Lin L, Yoshioka M, Yao Y, Shiraishi N (2006) Physical properties of moldings from liquefied wood resins. J Appl Polym Sci 55(11):1563-1571.

Ma XJ, Zhao GJ (2010) Preparation of carbon fibers from liquefied wood. Wood Sci Technol 44(1):3-11.

Maciá-Agulló JA, Moore BC, Cazorla-Amorós D, Linares-Solano A (2007) Influence of carbon fibres crystallinities on their chemical activation by KOH and NaOH. Micropor Mesopor Mat 101(3):397-405.

Masahiko K, Toshiyuki A, Mikio K, Bunichiro T (2004) Analysis on residue formation during wood liquefaction with polyhydric alcohol. J Wood Sci 50(5):407-414.

Mizuta K, Matsumoto T, Hatate Y, Nishihara K, Nakanishi T (2004) Removal of nitrate–nitrogen from drinking water using bamboo powder charcoal. Biores Technol 95(3):255-257.

Ngoc HP, Sebastien R, Catherine F, Laurence LC, Pierre LC, Thanh HN (2006) Production of fibrous activated carbons from natural cellulose (jute, coconut) fibers for water treatment applications. Carbon 44(12):2569-2577.

Olivares-Marín M, Fernández-González C, Macías-García A, Gómez-Serrano V (2006) Preparation of activated carbons from cherry stones by activation with potassium hydroxide. Appl Surf Sci 252(17):5980-5983.

Rong HQ, Liu ZY, Wu QL, Pan D, Zheng JT (2010) Formaldehyde removal by Rayon-based activated carbon fibers modified by *P*-aminobenzoic acid. Cellulose 17(1): 205-214.

Ryu Z, Rong H, Zheng J, Wang M, Zhang B (2002) Microstructure and chemical analysis of PAN-based activated carbon fibers prepared by different activation methods. Carbon 40(7):1144-1147.

Sing KSW, Everett DH, Haul RAW, Moscou L, Pierotti RA, Rouquerol J, Siemieniewska T (1985) Reporting physisorption data for gas/solid systems with special reference to the determination of surface area and porosity. Pure Appl Chem 57(4):603-619.

Tan IAW, Hameed BH, Ahmad AL (2007) Equilibrium and kinetic studies on basic dye adsorption by oil palm fibre activated carbon. Chem Eng J 127(1):111-119.

Uraki Y, Nakatani A, Kubo S, Sano Y (2001) Preparation of activated carbon fibers with large specific surface area from softwood acetic acid lignin. J Wood Sci 47(6): 465-469.

Yang R, Liu G, Li M, Zhang J, Hao X (2012) Preparation and N_2, CO_2 and H_2 adsorption of super activated carbon derived from biomass source hemp (*Cannabis sativa* L.) stem. Microporous Mesoporous Mater 158(1):108-116.